Geochemistry, Geophysics, Geosystems

AGU100 ADVANCING EARTH AND SPACE SCIENCE

GlobSed: Updated Total Sediment Thickness in the World's Oceans

E. O. Straume[1] iD, **C. Gaina[1]** iD, **S. Medvedev[1]**, **K. Hochmuth[2]** iD, **K. Gohl[2]** iD, **J. M. Whittaker[3]** iD, **R. Abdul Fattah[4]**, **J. C. Doornenbal[4]**, and **J. R. Hopper[5]** iD

[1]Centre for Earth Evolution and Dynamics, Department of Geosciences, University of Oslo, Oslo, Norway, [2]Alfred Wegener Institute, Helmholtz-Centre for Polar and Marine Research, Bremerhaven, Germany, [3]Institute for Marine and Antarctic Studies, University of Tasmania, Hobart, Tasmania, Australia, [4]TNO, The Geological Survey of the Netherlands, Utrecht, The Netherlands, [5]Geological Survey of Denmark and Greenland, Copenhagen, Denmark

Abstract We present GlobSed, a new global 5-arc-minute total sediment thickness grid for the world's oceans and marginal seas. GlobSed covers a larger area than previously published global grids and incorporates updates for the NE Atlantic, Arctic, Southern Ocean, and Mediterranean regions, which results in a 29.7% increase in estimated total oceanic sediment volume. We use this new global grid and a revised global oceanic lithospheric age grid to assess the relationship between the total sediment thickness and age of the underlying oceanic lithosphere and its latitude. An analytical approximation model is used to mathematically describe sedimentation trends in major oceanic basins and to allow paleobathymetric reconstructions at any given geological time. This study provides a much-needed update of the sediment thickness distribution of the world oceans and delivers a model for sedimentation rates on oceanic crust through time that agrees well with selected drill data used for comparison.

Plain Language Summary We have constructed a new global ocean sediment thickness map, GlobSed, from previously published maps and new data compiled in this study. GlobSed is used together with a new map of lithospheric ages developed for this study to analyze how sediment thickness changes with respect to the age of the underlying oceanic crust and latitude. The results show a clear age-latitude dependence where sediment thickness increases with age of the oceanic crust, toward high southern and northern latitudes and toward the equator. In addition, we calculate the total volume of sediments in the oceans, which shows an increase of 29.7%, compared to previously published global maps. Further, we develop a mathematical formula for sediment thickness as a function of age and latitude that describes the sediment thickness pattern in the oceans within reasonable error, and we suggest that this is a good approximation for estimating sediment thickness in oceanic basins through time.

1. Introduction

Knowledge of terrestrial and marine sediment thickness is critical to understanding geological evolution and processes. Globally, erosion and biogenic sedimentation followed by transport and deposition by wind or water determines the first-order structure of sedimentary accumulation. Subsequently, sediments can be tectonically deformed, redeposited or even subducted and therefore enter the deep-Earth cycle. Improved understanding of sediment thicknesses aids global studies in a wide range of subject areas, including analyses of thermal subsidence of the oceanic lithosphere (Crosby et al., 2006; Crosby & McKenzie, 2009), lithospheric thinning along continental margins (Crosby et al., 2011), or in paleobathymetric reconstructions (Goswami et al., 2015; Müller, Sdrolias, Gaina, Steinberger, et al., 2008).

On long geological timescales, the geology and geography of the continents and the world oceans are mostly controlled by plate tectonics. Most of the large oceanic basins have been formed due to seafloor spreading, a process initiated after continental lithosphere breakup. The oceanic lithosphere forms and subsides due to cooling—a process that is age dependent (e.g., Crosby & McKenzie, 2009; Parsons & Sclater, 1977; Stein & Stein, 1992) and is covered by various sediment types depending on the depth, proximity of continental margins, and interactions with the oceanic currents and biosphere. The depth of seafloor adjusts depending on sediment loading and isostatic response to that loading. Using this simplified relationship between the lithospheric age, thermal subsidence and depth, and the sediment accumulation history one can infer first-order approximations of ocean depths through time.
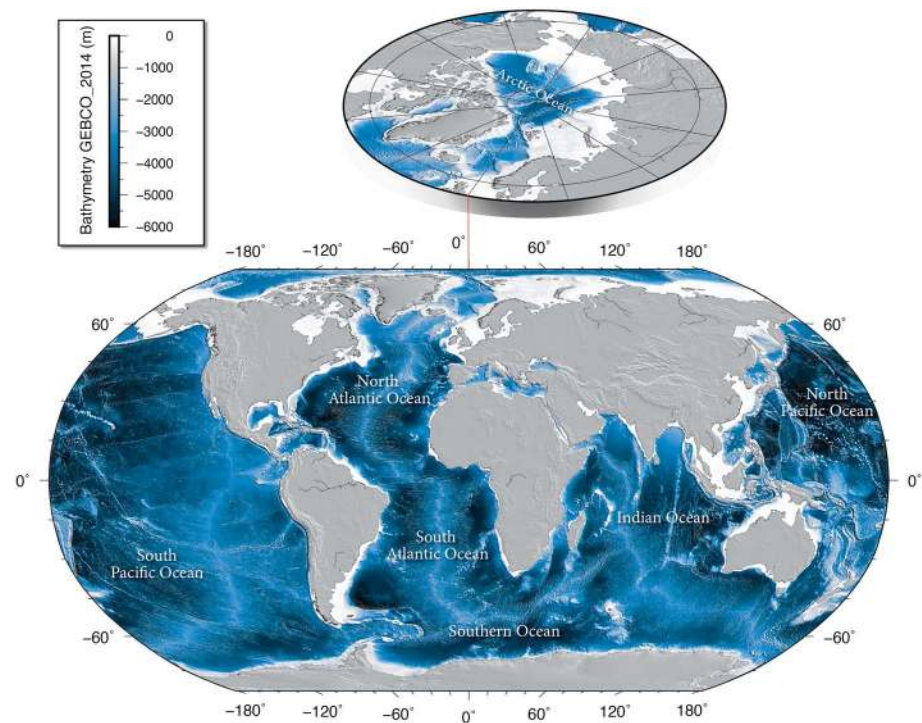
Figure 1. Global GEBCO_2014 bathymetry map (Weatherall et al., 2015) and a polar map of the Arctic Ocean.

In the last decade, several regional and global models of oceanic lithospheric age have been published (e.g., Müller, Sdrolias, Gaina, & Roest, 2008; Müller et al., 2016). Global compilations of sediment thickness are also available (e.g., Divins, 2003; Laske et al., 2013; Whittaker et al., 2013; Wobbe et al., 2014). However, due to uncertainties in some of the most used global sediment thickness compilations (Divins, 2003; Laske et al., 2013), some studies that used these compilations excluded sediment thickness >1.5 km as they observe that the uncertainty grows with greater sediment thickness (i.e., Crosby & McKenzie, 2009), while others excluded sediment thickness of poorly resolved areas along the continental margins (i.e., Crosby et al., 2011). The uncertainties in the global grids often results from the insufficient data coverage. Lack of seismic reflection/refraction profiles, especially in the deeper part of the ocean, causes uncertainties in sediment thickness independent of the grid node spacing in the digital maps (e.g., Divins, 2003; Whittaker et al., 2013). It is therefore important to continuously update the global compilations as new seismic data are collected.

Here we revisit the present-day distribution of sediments in the world oceans by considering recent and more accurate regional sediment thickness compilations in the Northern Hemisphere (the North Atlantic, the Arctic, and Mediterranean regions) and the Southern Ocean (Figure 1) and combine them with available global compilations (i.e., the NGDC and Laske et al., 2013 grids). The new total sediment thickness grid, GlobSed, is then analyzed together with our new model for the oceanic lithospheric age to derive first-order patterns in the global sediment thickness distribution and in selected ocean basins. Ultimately, we provide a much-improved present-day global distribution of total sediment thickness and a series of algorithms that can be used for reconstructing sediment thickness in oceanic basins through time.

2. Data and Global Compilation

Several regional oceanic sediment thickness maps have been recently compiled and published for the, (1) NE Atlantic (Funck et al., 2017; Hopper et al., 2014), (2) Mediterranean (Molinari & Morelli, 2011), (3) Arctic (Petrov et al., 2016), and (4) Weddell Sea (Huang et al., 2014). State-of-the-art global compilations of gridded data comprise new sediment thickness evaluation of the Southern Ocean in the Australia-Antarctica region (Whittaker et al., 2013) and the Ross Sea, Amundsen Sea, and Bellingshausen Sea sectors off West Antarctica (Lindeque et al., 2016; Wobbe et al., 2014). In this study, we merge the above-mentioned grids and updated
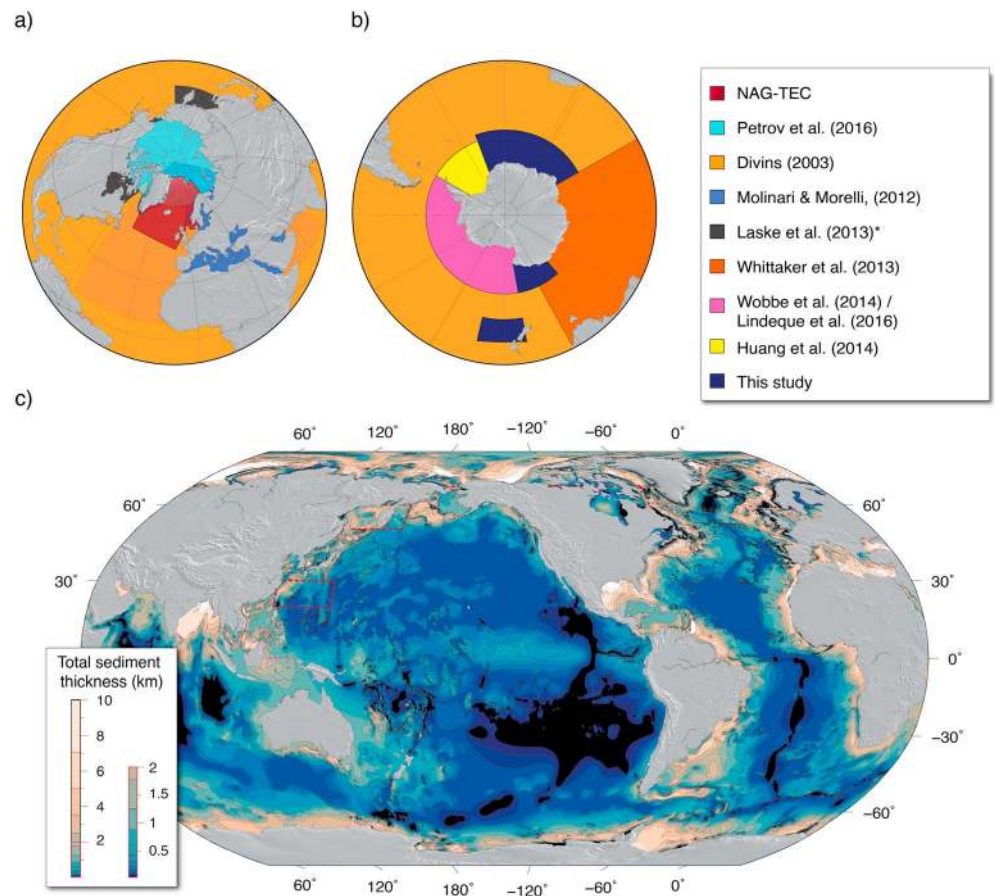
Figure 2. New global total sediment thickness grid, GlobSed. (a) Sources of the grids compiled to fill the previously poorly mapped Arctic and the NE Atlantic oceans and the Mediterranean Sea. Darker orange in the Northern Hemisphere indicates the full extent of the Molinari and Morelli (2012) grid, but it was only used in areas colored dark blue (e.g., in the Mediterranean Ocean). (b) Sources of the updated sediment thickness map of the Southern Ocean. See color legend and text for references. (c) Map showing total sediment thickness in kilometers. Regions inside red dashed polygons indicate sediment thickness values taken from the Laske et al. (2013) grid with an original coarser grid node spacing (1°) than the other used grids. This grid was given a lower priority in the grid merging order and is marked (*) in the color legend.

Southern Ocean and NE Atlantic compilation with the previous NGDC grid to produce a new total sediment thickness grid (Figure 2). The sediment thickness compilations used in this work will be further described below.

2.1. Total Sediment Thickness Data in the NE Atlantic

A new total sediment thickness grid of the NE Atlantic (Figure 3) was compiled for the international NAG-TEC project (Hopper et al., 2014). This grid was produced by combining several different compilations that covered subsets of the entire region (see Table 1 and supporting information Figure S1). Individual data sets were selected by quality checking all available sediment thickness data in the area, with a preference for the most recent data. In some areas, in particular east of Greenland, around Iceland, and around the Jan Mayen microcontinent, local maps and new interpretation of seismic reflection data were included (supporting information Figure S1 and Hopper et al., 2014). Over the continental margins and transitional areas, the total sediment thickness includes the entire cover sequence, which may include basalts and subbasaltic sedimentary rocks. This is due to difficulties distinguishing volcanic layers from sedimentary layers and may lead to a slight overestimation of sediment volume. In areas where very thick volcanic sequences are indicated, such as around the Jan Mayen microcontinent and Iceland, marginal areas with thick seaward dipping reflector sequences, and over oceanic crust, the top of basalt is used as depth to basement for sediment thickness. In these latter cases, sediment thickness may be underestimated where basalts have buried older sediments. After compiling all this information, there remained many large gaps, especially in oceanic areas (see
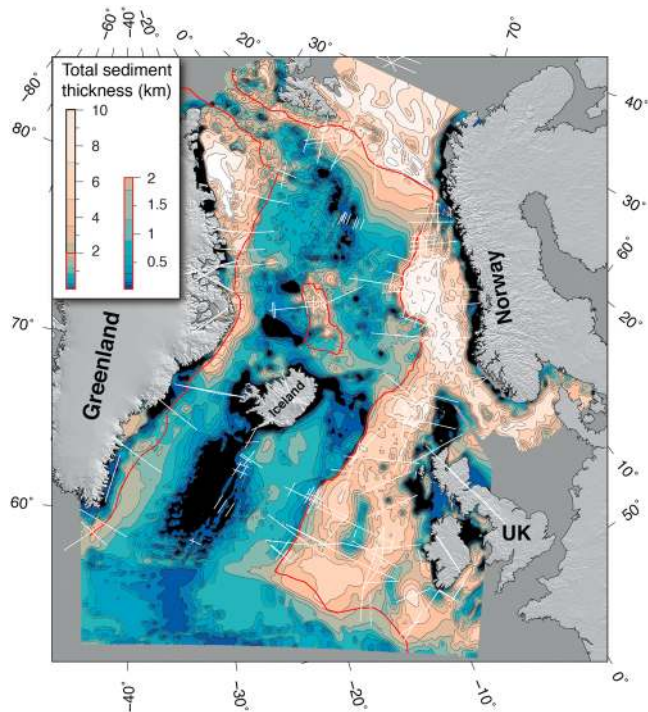
Figure 3. New NE Atlantic sediment thickness map used in the GlobSed grid. The red lines indicate the continent-ocean boundaries of Hopper et al. (2014). The white lines indicate the location of refraction seismic lines (Funck et al., 2017).

supporting information Figure S1). These areas were filled using the depth to basement grid based on regional seismic refraction (Figure 3 and Funck et al., 2017), which was produced using a gravity guided kriging technique. Individual data sets were resampled to 2 km before the map segments were stitched together. Further, the total sediment thickness was compared to well data and adjusted to ensure that sediment thickness is equal to or higher than observed in the wells, assuming that the wells have not penetrated the entire sedimentary sequence. To smooth the transitions between the individual gridded data sets and to avoid aliasing, the data were smoothed with five consecutive runs of a low-pass filter with 4-km diameter. The NE Atlantic sediment thickness grid (Figure 3) extends from ~50°N to the Fram Strait (about 82°N).

2.2. Updated Southern Ocean Sediment Thickness

We combined and updated the grid over the Southern Ocean (Divins, 2003), incorporating new data for the Australian-Antarctic corridor (Whittaker et al., 2013), the West Antarctic margin (Lindeque et al., 2016; Wobbe et al., 2014), and the Weddell Sea (Huang et al., 2014; Figure 4). We have modified the Weddell Sea data to include the results from seismic refraction experiments close to the edge of the ice shelf, which reveal deep sedimentary basins on the Weddell Sea shelf (Jokat & Herter, 2016). The sedimentary thickness for the Oates Land coast (170–150°E) as well as the Atlantic sector of the Southern Ocean (20°W to 50°E) has been reevaluated based on seismic reflection data (from Antarctic Seismic Data Library System SDLS, http://sdls.ogs.trieste.it/). The regional grid offshore New Zealand uses seismic reflection and refraction data acquired by the Alfred Wegener Institute and data provided by GNS Science, New Zealand (see Table 2). We used available velocity constraints from seismic refraction experiments (e.g., Jokat and Herter (2016), for the Atlantic sector and Grobys et al. (2007) for New Zealand), seismic stacking velocities and, if available, drill site information to convert seismic velocities to sedimentary thickness (e.g., Rogenhagen et al. (2004), and Huang et al. (2014) for the Atlantic sector and Horn and Uenzelmann-Neben (2015) for New Zealand). To combine the different data sets, we resampled them to 5-arc-minute grid spacing, and to ensure a seamless fit between the grids, we used overlapping grid regions to verify the comparability and consistency of the grids. A continuous surface tension was used during the gridding process (i.e., "surface," Generic Mapping Tools, Wessel et al., 2013).

2.3. Published Sediment Thickness Gridded Data and Grid Merging

The most recent global sediment thickness grid distributed by NCEI (the National Centers for Environmental Information, formerly known as the National Geophysical Data Center, NGDC) is the global 5-arc-minute grid of Whittaker et al. (2013). This global map covers most of the world's oceans, with exceptions of the Northern North Atlantic, Arctic, and Mediterranean Ocean and parts of the East China Sea and Sea of Okhotsk (Figure 2). The previous NCEI total sediment thickness of the world's oceans and marginal seas (Divins, 2003), was mainly compiled from published isopach maps (e.g., Divins & Rabinowitz, 1990;

Table 1

Available Total Sediment Thickness Data Sets Used to Cover the NE Atlantic Region

| Region	Compiler	Description	Year	Resolution
Norway	Ebbing and Olesen (2010)	Seismic, Magnetic and gravity data	2010	5 km
United Kingdom	BGS	Interpreted from gravity, seismic refraction and well data	2013	2 km
Greenland	GEUS/AWI	Interpretation of seismic reflection lines	2013	—
Iceland	ISOR	Local maps: Iceland Basin, North Iceland shelf, JMR, RR	2013	—
NE Atlantic	NAG-TEC	Interpreted from NAG-TEC database, guided by gravity data	2013	2 km
NE Atlantic	Oakey and Stark (1995)	Sediment thickness North Atlantic	1995	5 km
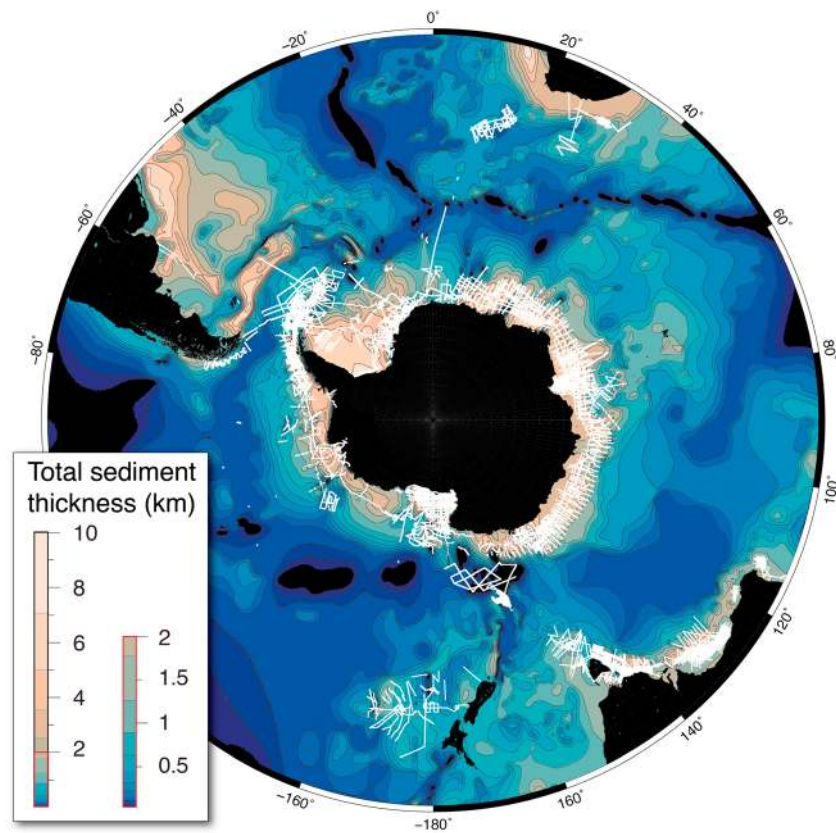
Figure 4. Southern Ocean total sediment thickness with locations of seismic lines (white lines).

Divins, 2003; Hayes & LaBrecque, 1991; Ludwig & Houtz, 1979; Matthias et al., 1988), drilling results from
the Ocean Drilling Program and Deep Sea Drilling Project, and seismic data as a part of the Intergovernment
Oceanographic Commission's International Geological-Geophysical Atlas (Udintsev, 2003) as well as seis-
mic reflection profiles of Divins (2003). The Whittaker et al. (2013) version was the second of the NCEI sedi-
ment thickness maps and included updates for the Australian-Antarctic region. The Whittaker et al. (2013)
compilation has been updated by Wobbe et al. (2014) and Lindeque et al. (2016) for the Ross Sea, Amundsen
Sea, and Bellingshausen Sea sectors off West Antarctica, but these updates have not been published by
NCEI. Another available global sediment compilation by Laske et al. (2013) is based on previously published
digital maps and hand-digitized grids from available maps and atlases.

Petrov et al. (2016) published a sediment thickness map for the Arctic inferred from available seismic data.
Regions of the Arctic lacking seismic data were filled by the global CRUST1.0 (1° × 1°) sediment thickness

Table 2
Available Total Sediment Thickness Data Sets Used to Cover the Southern Ocean Region

| Region	Compiler	Description	Resolution
Australia–Antarctica	(Whittaker et al., 2013)	Interpolation of seismic reflection lines	5 min
Ross Sea–Amundsen Sea–Bellingshausen Sea off West Antarctica	(Lindeque et al., 2016; Wobbe et al., 2014)	Interpolation of seismic reflection lines and well data	5 min
Weddell Sea	(Huang et al., 2014) (updated with Jokat & Herter, 2016)	Interpolation of reflection seismic lines augmented with refraction seismic results	5 min
Atlantic East Antarctic Margin 20°W to 50°E Oates Coast (170–150°E)	K. Hochmuth of this paper	Interpolation of seismic reflection lines (SDLS)	5 min
New Zealand	K. Hochmuth of this paper	Interpolation of seismic reflection lines	5 min
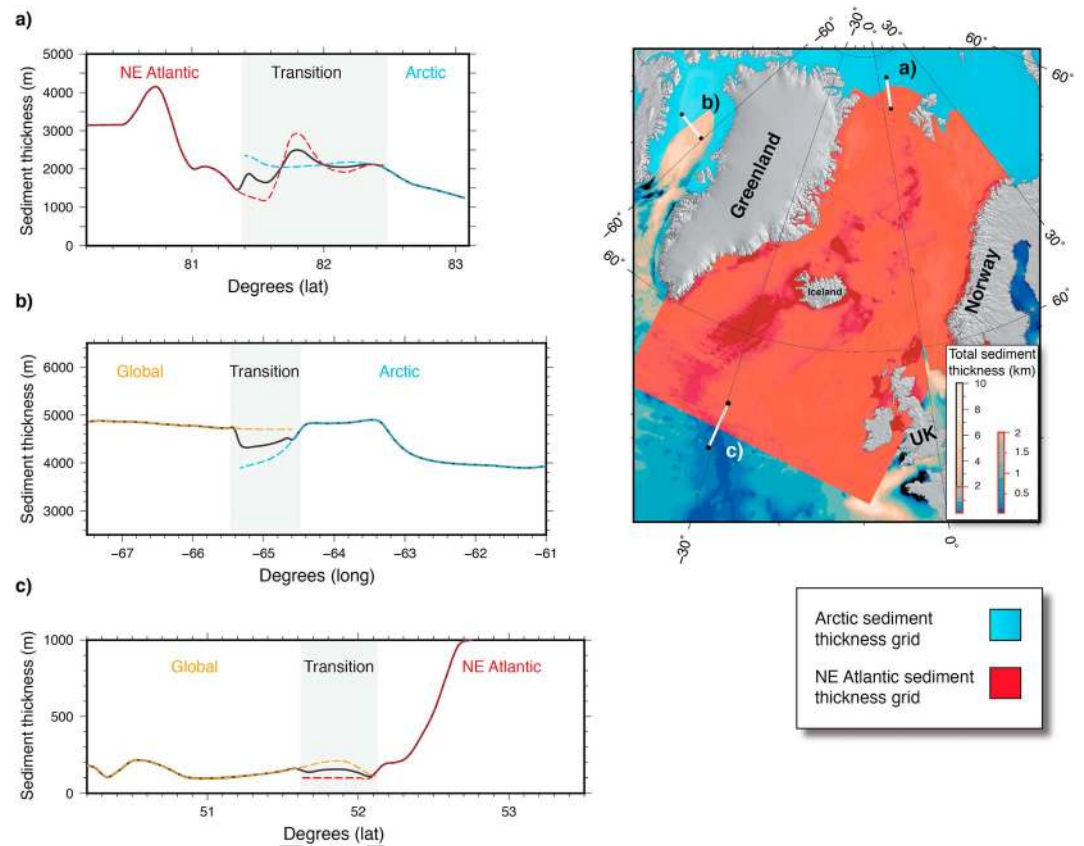
Figure 5. Selected profiles across areas where the contributed grids overlap and our solution for discrepancies. (a) Overlap of the NE Atlantic and the Arctic sediment thickness grids north of the Fram Strait. (b) Overlap of the semiglobal and Arctic sediment thickness grids in Baffin Bay. (c) Overlap of the Whittaker et al. (2013) and NE Atlantic grids in the North Atlantic Ocean. Dashed lines indicate grid values before merging, and black line shows values of the final combined grid.

grid of Laske et al. (2013; Petrov et al., 2016). For the GlobSed compilation, the Arctic sediment thickness by Petrov et al. (2016) been further checked and modified according to recent seismic reflection data in the eastern Eurasia Basin (e.g., Nikishin et al., 2017) and in the Barents Sea.

The combined modified Arctic (Petrov et al., 2016), the new NE Atlantic and the current NCEI global sediment thickness grids (Divins, 2003; Whittaker et al., 2013) cover most of the oceanic domain in the Northern Hemisphere; however, the Mediterranean Ocean, Baltic Sea, and some smaller regions were not enclosed. Therefore, we filled these regions (Figure 2) using the total sediment thickness grid from the European reference crustal model EPcrust (Molinari & Morelli, 2011). This grid contains data of the entire European plate, from North Africa to the North Pole and the Mid-Atlantic ridge to the Urals, with a grid cell spacing of $0.5° \times 0.5°$. Where EPcrust overlapped with the other grids (i.e., NE Atlantic, Arctic, or NCEI's total sediment thickness grids), the others were preferred as the quality and resolution of EPcrust is the least precise.

2.4. A New Global Sediment Thickness Grid

We merged the new and previously published sediment thickness grids described above, using the open-source software Generic Mapping Tools (GMT, Wessel et al., 2013). We combined overlapping grids by applying a weighting scheme in which the weighting of each grid formed a cosine taper with distance (using "grdblend," from the GMT tool box; Figure 5). Priority was given to the highest-resolution data. The lower-resolution data sets that overlapped spatially with the with other data sets were cut to avoid blending complications in the final global grid, leaving a narrow overlapping region (~1°) to ensure a smooth transition between the grids. Figure 5 shows three examples of grid merging. The NE Atlantic and Southern Ocean sediment thickness data were given the highest priority followed by the NCEI grid and the Arctic and EPcrust total sediment thickness grids. In the final compilation, sediment thickness information for some
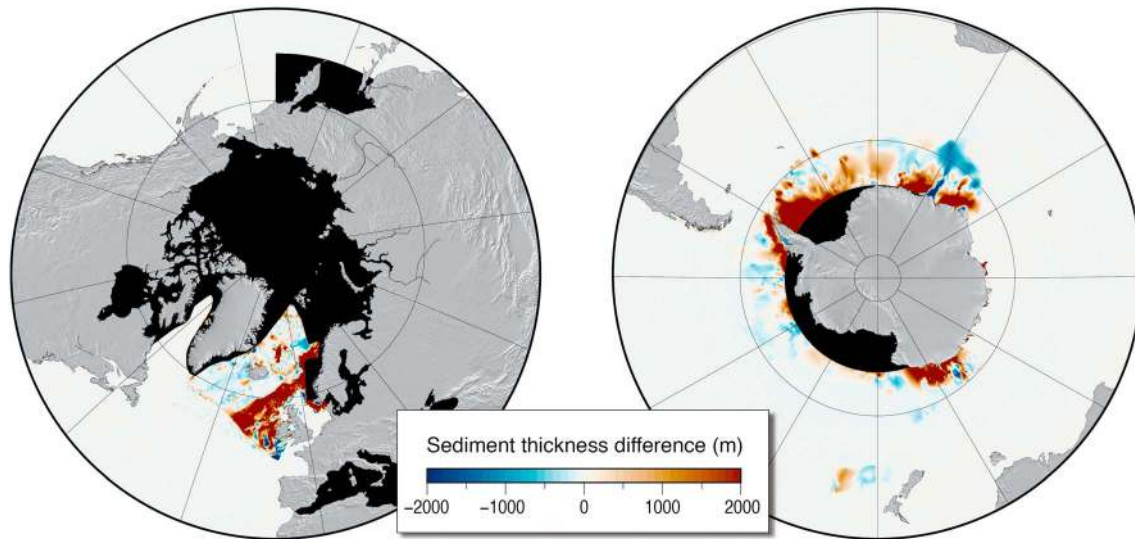
Figure 6. Polar maps showing the difference between the new total sediment thickness grid, GlobSed, and the sediment thickness grid of Whittaker et al. (2013). The black regions mark blank areas in the previous National Centers for Environmental Information grid, which are now covered by the GlobSed grid.

oceanic areas was still lacking (Figure 2), so we filled these regions with the 1° global grid of Laske et al. (2013). The difference between GlobSed and the previous NCEI's grid by Whittaker et al. (2013) is shown in Figure 6. The large difference in the circum-Antarctic region is due to the incorporation of previously unknown or unpublished seismic data. In particular, the Bellingshausen Sea and Amundsen Sea sectors of West Antarctica have only recently been surveyed by seismic profiling in a line distribution to generate sediment thickness grids (Lindeque et al., 2016; Wobbe et al., 2014). The first integrated analysis of sediment thicknesses and distribution in the Weddell Sea was performed by Huang et al. (2014). The same applied for the Arctic Ocean where numerous seismic survey lines have been acquired in the last 15 years.

2.5. Sediment Volume in the world's Oceans

GlobSed was used to calculate the total volume and mean thickness of the sediments in the world's oceans (see Table 3). We compute that there are ~3.37×10^8 km3 of sediments in the global ocean, ~10^7lkm3 km more than the total sediment volume estimated from the global grid of Whittaker et al. (2013). The new grid covers 7.4% more ocean area than the former grid and represents a sediment volume greater by ~29.7%. This is mostly due to our new constraints on the large sediment volumes in the Arctic Ocean, the Mediterranean Ocean, and the Weddell Sea. For comparison, LaRowe et al. (2017), calculated the total sediment volume to be ~3.01×10^8 km^3 based on earlier global compilations of sediment thickness (i.e., Laske, 1997; Whittaker et al., 2013).

Global oceans cover shallow continental areas that may extend tens or hundreds of kilometers from the coastlines and deeper abyssal plains. We consider here that oceanic crust floors the regions offshore the so-called continent-ocean boundary (COB), which is a simplified tectonic term we adopt here as the continentward boundary for what we call *oceanic basins*. We use the global COBs described by Torsvik and Cocks (2016) and a modified outline of back-arc basins from Matthews et al. (2016) for the SE Asia and SW Pacific. Globally, the continental shelves and the adjacent oceanic crust (here within 200 km from the COB) contain ~66.5% of the ocean sediments while only representing ~23.1% of the oceanic area. The continental margins alone represent ~12.9% of the oceanic area and contain more than 42% of the total sediment volume corresponding to a mean sediment thickness of 3,044 m, while the oceanic crust more than 200 km away from the shelves has an average sediment cover of 404 m.

Table 3
Volume, Area, and Mean Height of Sediments in the Oceans Calculated From the New and Previous Global Grids

Sediment thickness grid	Volume	Area	Mean thickness
This study	~3.37×10^8 km^3	~3.63×10^8 km^2	927 m
Deep ocean[a]	~1.13×10^8 km^3	~2.79×10^8 km^2	*404* m
Continental margins	~1.43×10^8 km^3	~4.69×10^7 km^2	*3,044* m
Whittaker et al. (2013)	~2.37×10^8 km^3	~3.36×10^8 km^2	705 m
LaRowe et al. (2017)	~3.01×10^8 km^3		721 m

[a]The deep ocean is defined as the area covering oceanic seafloor situated more than 200 km away from the continent-ocean boundary. Our calculations show that ~7.6×10^7 km^3 (~22.5%) of the sediments in the oceans lies on the oceanic crust less than 200 km away from the continent-ocean boundaries.
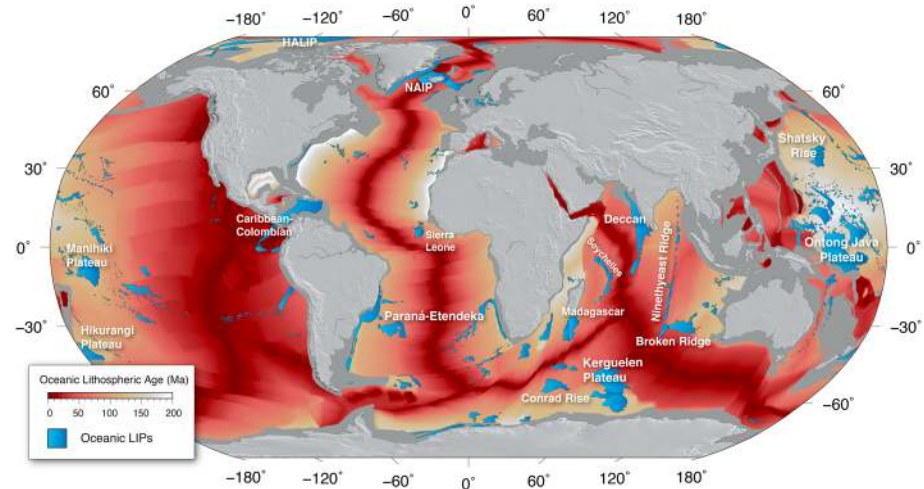
Figure 7. Age of the oceanic lithosphere (see text for details). Oceanic large igneous provinces from Torsvik and Cocks (2016) are colored in light blue. NAIP = North Atlantic Igneous Province; HALIP = High Arctic Large Igneous Province.

These very different sedimentary regimes control the biggest differences in sediment thickness in the oceans. For example, volumetrically ~40% of all sediments overlying oceanic crust is found within 200 km of a continental shelf, corresponding to ~22.5% of the total marine sediment volume (see Table 3). In section 3.3, we analyze the relationship between sediment thickness and age of the oceanic crust where caution is needed when accounting for oceanic regions near continental margins as they tend to accumulate much more sediments than the regions far away from the continents.

3. Age, Morphology, and Sediment Distribution on Oceanic Lithosphere

The sediment distribution in the world's oceans depends on many factors including the age of the oceanic lithosphere, the proximity to continental margins or large river discharge, oceanic current transport, and oceanic biological and chemical settings. Previous studies have shown that there is a direct correlation between the thickness of sediments deposited on oceanic lithosphere and the lithospheric age (e.g., Goswami et al., 2015; Müller, Sdrolias, Gaina, Steinberger, et al., 2008). Here we use a similar approach (section 3.3) using GlobSed and an updated model of global oceanic lithospheric age for estimating sediment thickness distribution with respect to the age of the oceanic lithosphere.

3.1. Age of the Oceanic Lithosphere

Our gridded oceanic crustal ages (Figure 7) are based on an improved database of magnetic anomaly identi- **F7** fications that were modeled as described by Müller, Sdrolias, Gaina, and Roest (2008) using the geomagnetic polarity timescale of Ogg (2012). The presented oceanic lithospheric age model builds on the Seton et al. Q9 (2012) global model and includes recent regional plate tectonic models of the African plate, Indian Ocean, NE Atlantic, and the Arctic (Gaina et al., 2013, 2015, 2017, respectively, Nikishin et al., 2017) and a revised, more detailed global model for Eocene age oceanic lithosphere (Gaina & Jakob, 2018). The computation of age of oceanic lithosphere considers the formation of "normal" oceanic lithosphere through seafloor spreading. However, many large bathymetric features seen in the world's bathymetric map (Figure 1) were not formed by normal seafloor spreading processes, most of these being related to emplacement of additional volcanic material at the time or after oceanic crust formation. These regions include large igneous provinces (LIPs), which may have been formed due to the arrival of deep-rooted mantle plumes at the base of the lithosphere causing massive volcanic eruptions over geologically short periods (e.g., Coffin & Eldholm, 1994; Morgan, 1971; Torsvik et al., 2006; Torsvik & Cocks, 2016). These anomalous large-scale bathymetric features are known to control ocean currents directions and induce contourite drift deposits and erosion (e.g., Dutkiewicz, Müller, et al., 2016; Rebesco et al., 2014), yielding anomalous sediment thickness compared to normal seafloor. For our analysis (section 3.3), we remove the oceanic areas where LIPs (locations and outlines from Torsvik & Cocks, 2016) were emplaced in order to avoid the bias toward a different style of
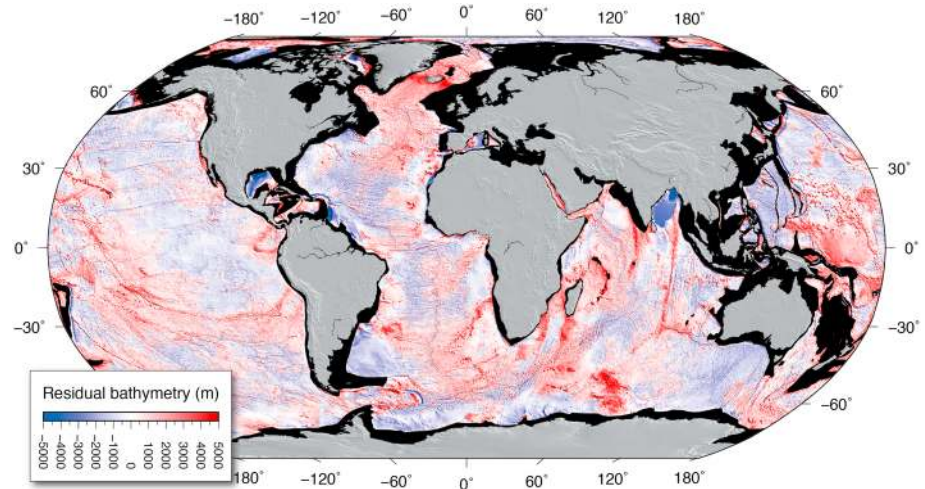
Figure 8. Global residual bathymetry of the oceanic lithosphere.

sedimentation than the one linked to the steady sedimentation on a gradually aging and subsiding oceanic crust. The importance of LIPs for global bathymetry will be discussed in the next section.

3.2. Residual Bathymetry

To identify regions of the world's oceans where processes other than normal seafloor spreading have contributed to bathymetry, we compute the global residual bathymetry (Figure 8), defined here as the difference **F8** between the predicted depth to basement according to thermal subsidence of normal oceanic lithosphere and the observed sediment unloaded basement depth. To compute the oceanic lithosphere thermal subsidence, we use the Crosby and McKenzie (2009) formula:

$$d = \begin{cases} -2,652-324\sqrt{\tau} & \tau \leq 75\text{Ma} \\ -5,028-5.26\tau + 250\sin\left(\dfrac{\tau-75}{30}\right) & 75\text{ Ma}<\tau \leq 160\text{ Ma} \\ -5,750 & \tau > 160\text{ Ma} \end{cases} , \qquad (1)$$

where d is the basement depth in meters and τ is the age of the oceanic lithosphere in million years. Since equation (1) was derived excluding regions with anomalous crustal thickness, the prediction is considered suitable for detecting anomalies in basement depth caused by, for example, hot spot-related swells, seamounts and oceanic plateaus (Crosby & McKenzie, 2009; Wobbe et al., 2014). To calculate the sediment unloaded basement depth, we subtracted the sediment thickness from the present-day bathymetry GEBCO_2014 (Weatherall et al., 2015) and applied the isostatic correction method of Sykes (1996). In the resulting residual basement depth, there are several distinctive features (Figure 8). For example, oceanic LIPs (e.g., Ontong Java Plateau, Kerguelen Plateau, Shatsky Rise, and Greenland-Iceland-Faroe Ridge) are associated with positive residual bathymetry (Figures 7 and 8). This is also true for seamounts, and most of the NE Atlantic where the large positive residual bathymetry may be the result of increased igneous crustal thickness and dynamic topography of the Iceland Plume swell (Jones et al., 2002). Many negative anomalies are associated with subduction zones (Figure 8), as they are deeper than predicted by normal thermal subsidence of oceanic lithosphere. For other negative anomalies, like in the Bay of Bengal, the residual bathymetry is related to the highly anomalous thick sedimentary cover.

3.3. Analysis of Sediment Thickness Distribution in Global Oceanic Basins

Many mechanisms and factors control sediment accumulation on the ocean floor. Here we analyze how present-day sediment thickness distributed on oceanic crust is related to global parameters such as latitude and seafloor age. We attempt here to derive a simple crude model of the sediment cover of the normal crust, the crust that is unaffected by regional and local perturbations. We exclude oceanic plateaus and other anomalous regions with very high or very low (±5,000 m) residual bathymetry (section 3.2, Figure 8) and
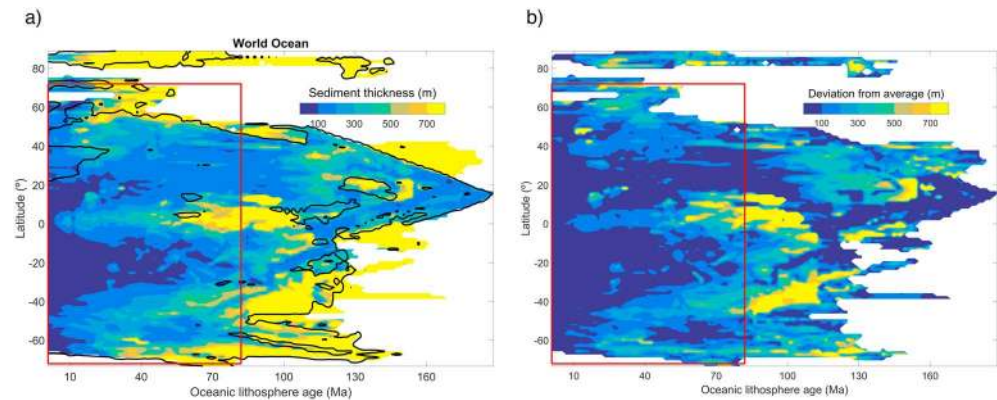
Figure 9. Values of average sediment thickness (a) and standard deviation (b) for considered sediment data (see text for details of excluded data) distributed over bins 1.5 Myr by 1.5° of latitude. Black line in (a) cuts out areas with few data (less than 130 data in each bin). Red rectangle outlines area considered in more detail.

areas characterized by highly anomalous sediment thickness (the Mediterranean and Arabian Seas and the Bay of Bengal). We also exclude areas within 200 km of the continental margins.

We separate the seafloor age and latitude space into bins of 1.5 Myr of age and 1.5° of latitude and analyze sediment thickness data within each bin. We first consider distribution of sediment thickness by calculating standard deviation (STD) within each bin and exclude outliers where sediment thickness differs more than 1.8 STD from the average value, resulting in 4.5% of data points excluded. We then calculated the average value for each bin. Figure 9a displays the distribution of average sediment thickness in the age-latitude space, which will be used in the further analysis. Figure 9b demonstrates that the average values shown in Figure 9a are reasonably representative as the STD calculated for each bin (average 209 m) is smaller than the average value in most of the bins (average total 586 m), although the accuracy of such representation is limited.

Although, ideally, data would be analyzed over as large a range as possible, the data at high latitudes and for older ages are limited. The uncertainty of age estimations increases for ocean lithosphere >83 Myr old. Thus, the following analysis excludes latitudes higher than 72°S and N and age greater than 82 Myr (red rectangle in Figure 9a). This younger part of the ocean is characterized by an average sediment thickness of 267 m with average STD of 140 m. The STD value is rather high because the total analysis includes several oceans. Thus, we present the same analysis for each ocean separately (Figure 10) which resulted in average STDs smaller than one third of the average sediment thickness for each ocean, although the average thickness of sediments is different.

The results presented in Figures 9 and 10 agree with previous findings that sediment thickness increases with age of the oceanic lithosphere (e.g., Olson et al., 2016). In addition, our analysis confirms that sediment
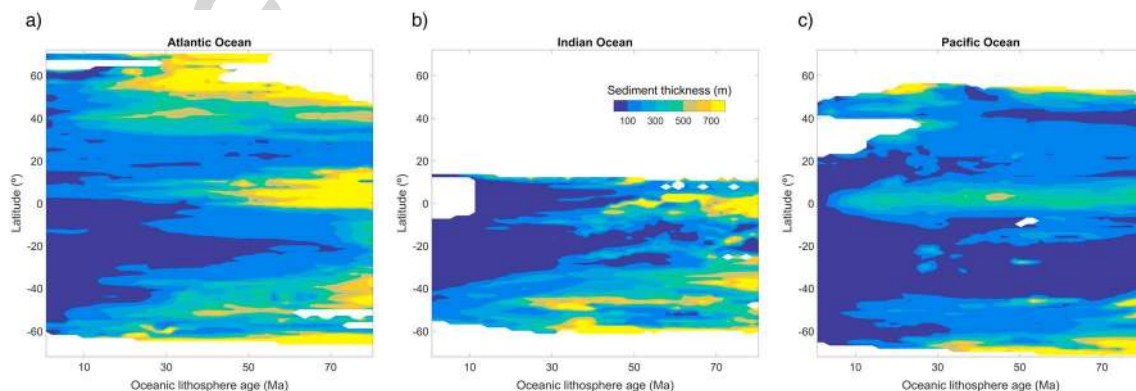

Figure 10. Distribution of average sediment thickness for Atlantic (a), Indian (b), and Pacific (c) Oceans. The data analysis is restricted to maximum 82-Ma age of the oceanic lithosphere and up to 72° of latitude (north and south).
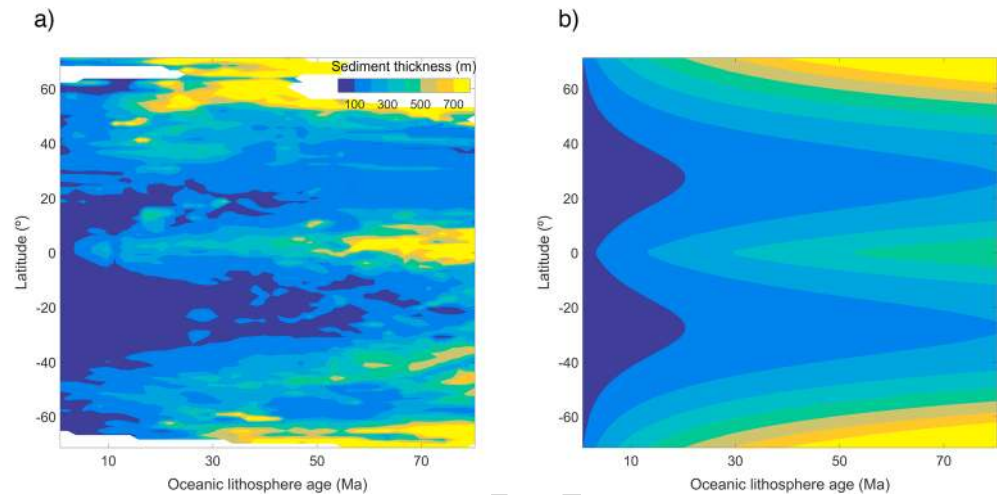
Figure 11. (a) Distribution of average sediment thickness in world's ocean for the parameter space restricted by the red rectangle in Figure 9. (b) Analytical approximation of the average sediment thickness described by equation (2).

thickness is also latitude dependent, showing an increase along equator and toward high latitudes. This relationship is valid for global sediment thickness (Figures 9a and 11a) and for individual oceans considered in this study (Figure 2).

The clear and simple trends of the sediment thickness distribution, such as thickness increased with age, along the equator, and toward the higher latitudes, lead us to consider an analytical representation of sediment thickness. Our task here was to find an analytical function, as simple as possible, that reasonably approximates our data. Goswami (2015) and Olson et al. (2016) approximated sediment thickness by cubic polynomial of oceanic lithosphere age by excluding oceanic lithospheric ages of 120 Myr and older. Our selected age range is reduced for reasons outlined earlier. The approximation derived here is a single term that depends on the square root of age, $\sqrt{\tau}$ (see also equation (1)) that works equally well as a cubic polynomial in the chosen age range. The latitude dependence is nonmonotonic but can be assumed as symmetric about equator. Thus, we use an absolute value of latitude λ instead of signed latitude values. The resulting dependence consists of three coefficients and is optimized using a least squares method:

$$Z(\lambda, \tau) = \sqrt{\tau}\left(c_1 + c_2\lambda + c_3\lambda^2\right), \tag{2}$$

$$Z(\lambda, \tau) = \sqrt{\tau}\left(52 - 2.46\lambda + 0.045\lambda^2\right), \tag{2a}$$

where Z is approximated sediment thickness in meters, τ is the oceanic lithosphere age in mega annum, and λ is the absolute value of latitude in degrees (distance to equator in degrees). Any further noticeable improvement of equation (2) would require at least a seven-term polynomial (see supporting information).

3.4. Robustness of the Sediment Thickness Distribution Models

Sediment thickness distribution is slightly asymmetric about the equator (Figure 11a). This asymmetry may be caused by asymmetric distribution of land mass, plate tectonic kinematics, uneven data quality, or geo-bio-climatic-physical processes. However, because of the complexity of these causes impacting global oceanic sedimentation, we will test only the hypothesis that the sediment accumulation conditions are the same on both hemispheres for our analytical approximation models (Figure 11b and Table 4).

To test the models in this section (Table 4), we compute the root-mean-square (RMS) difference between the postulated age-latitude-sedimentation model and the data (Table 4). To avoid domination by extreme values in estimation errors, we remove data points with sediment thickness more than 1.3 km. We first consider the global models (Figure 11) presented in the last row of Table 4 ("world ocean"). The main global analytical model (Figure 11b, RMS$_3$, equation (2) with coefficients in the right bottom of Table 4) naturally gives larger error than the nonanalytical average-bin model (Figure 11a, RMS$_1$) but shows sizable improvement if compared to the analytical model, which is based on age only (as suggested by Goswami (2015) and Olson et al.

Table 4
Comparison of Models With Compiled Sediment Thickness Data (RMS in meters)

Ocean	Average sediment thickness Z_{av}	Global model			Global model adjusted		Local models			
		RMS_1 Figure 11a	RMS_2 age	RMS_3 Figure 11b	RMS_4	k	RMS_5 equation (2)	C_1	C_2	C_3
Atlantic	273	206	252	228	222	1.29	219	57.98	−2.33	0.048
Indian	238	174	214	196	191	1.12	186	43.35	−1.41	0.034
Pacific	155	112	178	155	135	0.68	132	47.79	−2.54	0.044
World	196	136	199	177	—	1	—	53.02	−2.46	0.045

Note. RMS_1–RMS_5 are the root-mean-square errors for the (1) nonanalytical average bin model, (2) the analytical model based on age only, (3) the main global analytical model, (4) the main global analytical model scaled for the different ocean basins, and (5) regional analytical model built for each ocean separately.

(2016), RMS_2). A computation of sedimentation based on our global model sediment thickness formula for three selected oceans shows the same relation, $RMS_2 > RMS_3 > RMS_1$, demonstrating the impact of latitude dependence of sediment thickness.

The regional application of the analytical model (i.e., for the Atlantic Ocean, Pacific Ocean, and Indian Ocean) can be improved in two ways. We first compare the average sediment thickness of chosen data sets of the different ocean basins, Z_{av}, and scale equation (2) $Z_{local} = k \cdot Z_{world}$, where k is the ratio of the local to world's Z_{av}. This yields RMS_4, which is $<RMS_3$, and thus an improvement of the analytical model, especially for the Pacific Ocean. A second way to build a regional analytical model is to optimize equation (2) for each ocean separately. The models derived this way are presented in the last four columns of Table 4. This yields RMS_5, which does not show significant improvement of the adjusted global model (RMS_4). These results quantitatively support the observation that the sediment thickness trends of the world ocean are similar in the three selected oceanic basins. The quantitative differences between oceans, expressed via variations of parameter k, require additional analysis of sedimentation processes for each ocean but is beyond the scope of this study. The robustness of our analytical approximation can be also illustrated by the low difference between local coefficients of equation (2) (top three rows, last three columns in Table 4) and the world ocean coefficients. Note that coefficients in the model of Olson et al. (2016) differ by almost an order of magnitude for different oceans. In general, RMS values (Table 4) are comparable with the average values of the sediment thickness, reflecting great variations of sediments in oceans and limiting the predictive power of our analytical estimation. However, the strength of our analytical approximation equation (2) is in predicting the trends of the global sediment accumulation and can be used as a first approximation.

4. Discussion

4.1. Sediment Thickness Controlling Factors

There are numerous factors controlling sediment distribution in different ocean basins; among them are the tectonic history, age of the oceanic basin, structural trends in the basement including mid-ocean ridges, fracture zones, the nature and location of sediment sources, preglacial and glacial transport and deposition, ocean circulation, and chemical composition (e.g., Divins, 2003; Dutkiewicz, Müller, et al., 2016; Dutkiewicz, O'Callaghan, et al., 2016; Olson et al., 2016). Describing the sediment thickness distribution in the oceans as dependent on only two variables (age and latitude) is a simplification; however, they seem to show consistent trends with global sediment distribution in global oceans (Müller, Sdrolias, Gaina, Steinberger, et al., 2008; Olson et al., 2016). Increasing sediment thickness with increasing oceanic lithosphere age has been suggested and demonstrated before (Divins, 2003; Goswami et al., 2015; Olson et al., 2016). However, our analysis shows that the sediment thickness also largely depends on latitude, globally and separately in the three main oceanic basins, where we see a clear increase in sediment thickness toward equator and toward the high latitudes. The equatorial sediment bulge may arise from higher productivity of pelagic organisms due to oceanic upwelling along equator that cause the accumulation of thick calcareous and siliceous ooze (Mitchell et al., 2003; Mitchell & Lyle, 2005). In the Pacific, the equatorial bulge is actually positioned slightly north of the equator (Figure 2), probably as the northward component of the moving Pacific plate displace this sediment anomaly after deposition (Mitchell et al., 2003; Mitchell & Lyle, 2005). Generally, the observed sediment thickness-latitude relationship resembles the pattern of chlorophyll in the global ocean. The chlorophyll pattern indicates desert-like subtropical gyres and fertile equatorial, and

high northern and southern latitudes, seen from satellite-derived surface patterns and maps accounting for the vertical distribution of chlorophyll (e.g., Silsbe & Malkin, 2016; Uitz et al., 2006). This may indicate that higher biogenic productivity in these regions have been fairly stable through time and is an important factor for our observed latitude dependence of sediment thickness. Our use of absolute values of latitude in the analytical approximations (section 3.4) makes a symmetric pattern around equator, which would be expected if climate was the only factor controlling sediment thickness. However, plate tectonic-induced motions influence the latitude approximation since the plates are not fixed in time spatially. A more thorough analysis by implementing plate tectonic scenarios for individual ocean basins is beyond the scope of this paper, but our sediment thickness compilation opens the potential for future studies on geodynamic-tectonic-sedimentation ice sheet dynamics relationships. Also, sedimentation from large rivers may disturb the symmetric pattern, although the largest deltas overlying oceanic crust were removed from our analysis (see section 3.3).

The different oceanic basins all portray the same trends in sedimentation with lithospheric age and latitude; however, the average sediment thickness is higher in the Atlantic and Indian oceans compared to the Pacific Ocean. In section 3, equation (2) was scaled by a constant for the local basins, which improves the RMS values, especially for the Pacific Ocean. In contrast to the Indian and Atlantic oceans, which are flanked by passive continental margins, most of the Pacific Ocean, apart from its passive West Antarctic margin, is surrounded by active continental margins that allow sediments to accumulate in the accretionary wedges of the subduction zones and therefore inhibit transport of detrital sediments carried by avalanches or turbidity currents from reaching the abyssal planes. This could be part of the explanation why the sediment thickness is considerably lower in the Pacific compared to the other ocean basins. However, there are many factors controlling basin-scale pelagic sedimentation (such as internal waves, deep sea flow, sediment erosion and deposition related to topography, and dissolution of carbonate by ocean atmosphere interactions or subsidence of the seafloor, see Tominaga et al. (2011) and references therein) that may contribute to the sediment thickness differences we observe between the different ocean basins.

We find a strong relationship between sediment accumulation and latitude. Even though highly glaciated regions were excluded in the analysis (i.e., the northern North Atlantic and the Arctic Ocean and the Southern Ocean), the analytical approximations still show an increase in sediment thickness with higher latitudes (Figure 11b). The high sediment thicknesses of the Southern Ocean around the Antarctic margins are expected due to immense glacially driven deposition. But the thickness variations and large sediment accumulations in regions where low glacial outflow would not imply large sediment deposition are surprising and probably caused by strong shelf-parallel bottom currents redistributing fine-grained sediments.

4.2. Reliability of our Gridded Data Based on Observations From Scientific Drilling Sites

We compare our gridded data against 26 Deep Sea Drilling Project and Ocean Drilling Program sites in the Indian Ocean, where we take advantage of results from Sykes et al. (1998) who compiled information on sediment thickness, bathymetry, and age of the oceanic lithosphere (Figure 12). A good match, although **F12** with some outliers, is observed between the drill site sediment thickness and GlobSed (Figure 12a). The outliers may result from rugged topography of the oceanic crust, which could potentially cause large differences in sediment thickness over distances shorter than the grid resolution but also inaccuracies in the gridded data. Our modeled age of the oceanic lithosphere correlates well with the dated samples from the drill sites (Figure 12b). We do not see a perfect one-to-one correlation, which may partly be influenced by inaccuracies in dating, as some of the drill site ages are based on the oldest sediment age (Sykes et al., 1998). However, this is not significant as seen from Figure 12b, the scatter of data may rather suggest that random uncertainty dominates. A more detailed description of the individual drill sites, including correlations with 10 drill sites in the NE Atlantic Ocean can be found in the supporting information.

4.3. Toward Paleobathymetric Models Using Sediment Thickness-Lithospheric Age-Latitude Relationship

The analytical approximation of sediment thickness versus age and latitude (section 3.4) can be used for analysis and reconstruction of regional and global (paleo) bathymetry. As sediment thickness is difficult to precisely quantify back in time, formulas like equation (2) provide an approximation of how much sediment thickness can accumulate on "normal" oceanic lithosphere through time. The equation can be also used
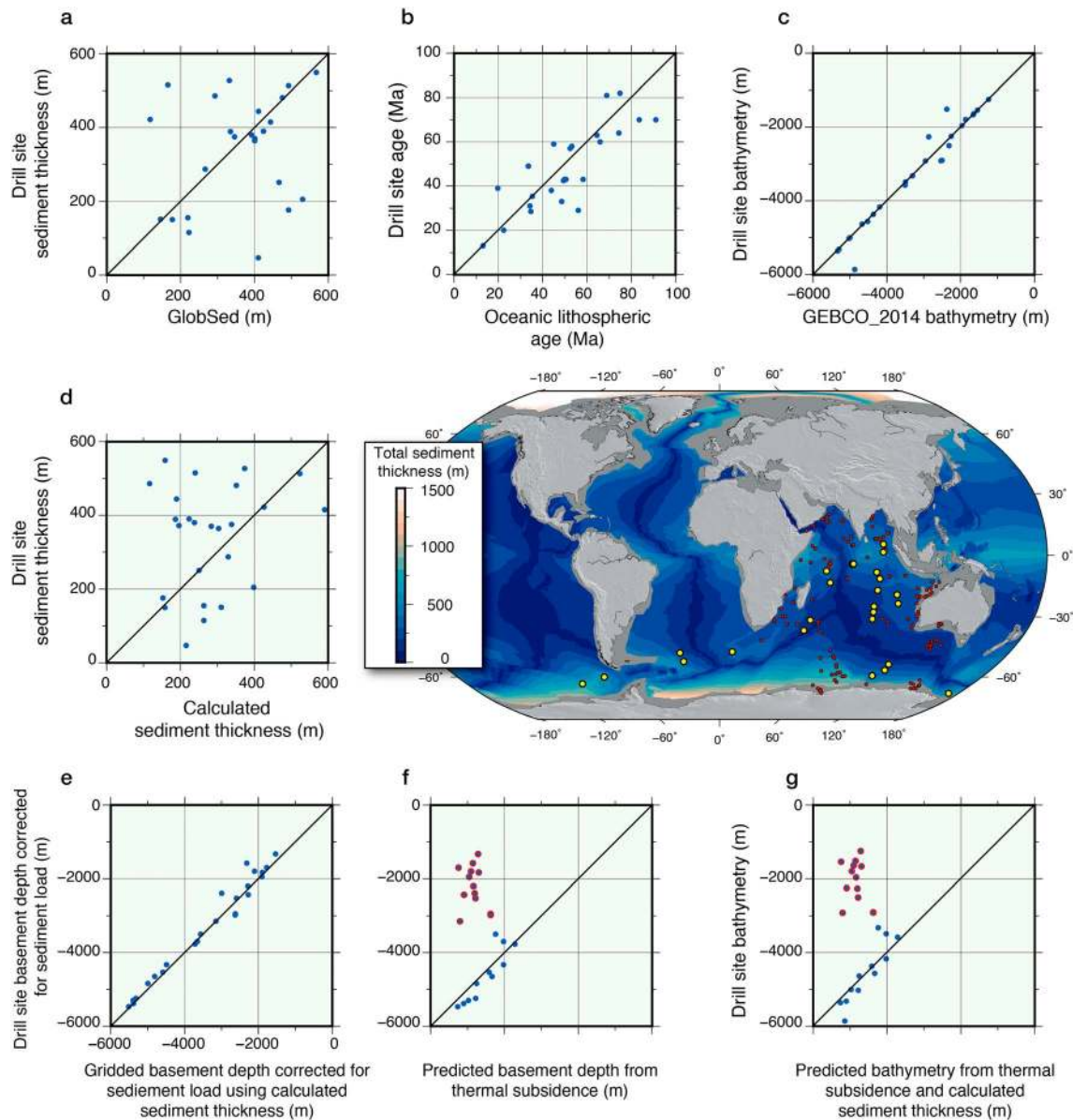
Figure 12. Drill sites (DSDP and ODP) in the Indian Ocean and few Southern Ocean locations plotted versus gridded and calculated data, each shown with a 1:1 linear regression line. Central map shows predicted sediment thickness using equation (2) (section 3.4). The location of drill sites used by Sykes et al. (1998) and for comparison with our results are shown in yellow on the map. For reference, we show all other DSDP/ODP/IODP sites in the Indian Ocean (red circles). (a) Sediment thickness recovered in selected drill sites versus the newly compiled global gridded sediment thickness. (b) Basement age from drill sites versus age grid model of oceanic crust. (c) Drill site bathymetry plotted versus GEBCO_2014 bathymetry. (d) Sediment thickness recovered in selected drill sites plotted versus calculated sediment thickness, using the formula for sediment thickness younger than 82 Ma. (e) Drill site basement depth corrected for isostatic effect of overlying sediments (Sykes et al., 1998) versus isostatically corrected basement depth using the newly calculated sediment thickness. (f) Isostatically corrected drill site basement depth plotted versus the predicted basement depth using the thermal subsidence formula of Crosby and McKenzie (2009). Red circled sites are located on anomalous oceanic lithosphere (e.g., oceanic plateaus; see section 4.2 for explanation). (g) Drill site bathymetry plotted versus modeled present-day bathymetry (calculated using thermal subsidence curve of Crosby and McKenzie (2009) and calculated sediment thickness using equation (2) (see section 4.3 for explanations).

to detect abnormalities in modern bathymetry and therefore help identify other processes than thermal subsidence. To test the accuracy of our formulas, we first calculate the predicted present-day global bathymetry. Using the lithospheric age grid and the formulas of Crosby and McKenzie (2009; see section 3.1), we calculate the predicted subsidence for normal seafloor (i.e., lithosphere not associated with previous LIP formation, subduction zone, or currently active hot spot). Then we calculate sediment thickness using equation (2) and correct for sediment loading by applying the isostatic correction formula of Sykes (1996). The calculated bathymetry correlates well with several of the drill site measured
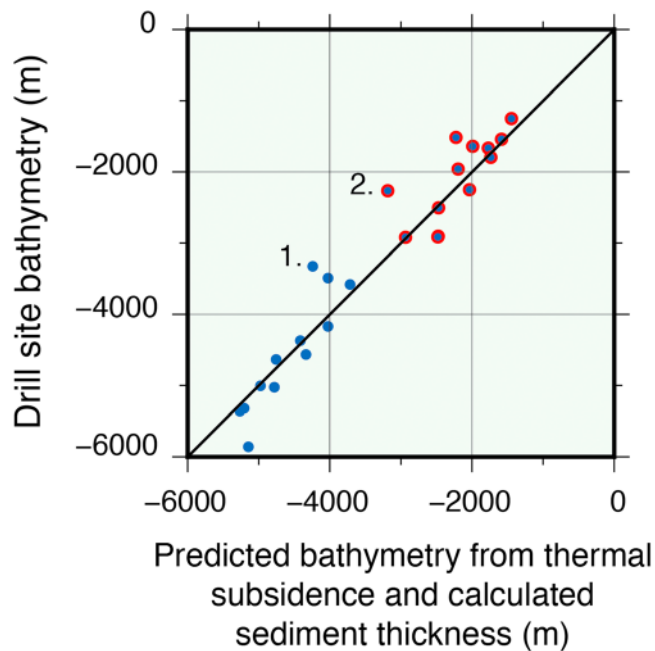
Figure 13. This is the same as in Figure 12g updated for residual bathymetry of large igneous provinces. See text for a more detailed explanation and supporting information for the outliers marked 1 and 2.

bathymetry (Figure 12g). Basement and bathymetric depth of a second group of drill sites is shallower than modeled (red circles in Figures 12f and 12g). Indeed, the anomalous sites are located on oceanic plateaus and cannot be explained by formulas derived from a data set that excludes such anomalous regions (a more detailed description of the specific drill sites can be found in the supporting information). To include anomalous bathymetry of LIPs in our global model, we add their residual bathymetry (calculated in section 3.2) to the initial bathymetric model that considers only thermal lithospheric subsidence, sedimentation rates, and isostasy. Figure 13 shows how this addition to the model significantly improves the comparison between modeled and observed bathymetry. The residual bathymetry of LIPs mostly reflects increased crustal thickness. Thus, subsequent thermal subsidence through time will follow the same trend as the underlying oceanic lithosphere as indicated by Schubert and Sandwell (1989). With this assumption, the depth of oceanic plateaus can be estimated in time and used for paleobathymetric reconstructions.

5. Conclusions

We present a new global total sediment thickness grid (GlobSed) that incorporates updated data from the NE Atlantic, Arctic, Mediterranean, and Southern Ocean regions. This grid, and an updated oceanic lithospheric age grid, have been used to calculate the residual bathymetry of the oceanic lithosphere, here defined as the difference between the bathymetry predicted by thermal subsidence (i.e., Crosby & McKenzie, 2009) and the observed sediment unloaded bathymetry. The residual bathymetry plot highlights anomalous regions such as oceanic plateaus and seamount-littered regions. An analysis of the thickness of oceanic sediments demonstrates a dependence on latitude and oceanic lithosphere age and shows a clear increase in sediment thickness with lithospheric age and toward the equator and high latitudes. These trends characterize the world's oceans as a whole and are also evident in the three major oceans individually (i.e., the Pacific Ocean, Atlantic Ocean, and Indian Ocean). Our analytical approximation model can be used to mathematically describe these trends (equation (2)) and construct models that can be used to reconstruct paleobathymetry at any given geological time. The sediment thickness in the Pacific Ocean differs from the other ocean basins as it has lower average sediment thickness. In contrast to the Atlantic and Indian oceans, most the Pacific Ocean, with exception of its passive West Antarctic margin, is surrounded by active margins, which may play a role governing the differences in sediment distribution. We were able to scale our global analytical approximation by a constant value and yield better correlation between model and data for each ocean basin, especially in the Pacific Ocean. However, finding particular sources of different bulk sediments in each ocean and understanding the quantitative adjustment are beyond the scope of this study. To test the validity of the calculated and gridded data, information from 26 drill sites in the Indian Ocean and 10 drill sites from the NE Atlantic Ocean were compared to the sediment thickness model. This comparison shows an overall good correlation. Further, we compared GEBCO_2014 bathymetry with that calculated using the formula of Crosby and McKenzie (2009) and the sediment thickness formula for crustal ages younger than 82 Ma. We obtain a good match between the calculated and observed bathymetry, which demonstrates the robustness of using such formulas in paleobathymetric reconstructions.

References

Coffin, M. F., & Eldholm, O. (1994). Large igneous provinces: Crustal structure, dimensions, and external consequences. *Reviews of Geophysics*, *32*(1), 1–36. https://doi.org/10.1029/93RG02508
Crameri, F. (2018a). Geodynamic diagnostics, scientific visualisation and StagLab 3.0. *Geoscientific Model Development*, *11*(6), 2541–2562. https://doi.org/10.5194/gmd-11-2541-2018
Crameri, F. (2018b). Scientific colour-maps. https://doi.org/10.5281/zenodo.1243862
Crosby, A., McKenzie, D., & Sclater, J. (2006). The relationship between depth, age and gravity in the oceans. *Geophysical Journal International*, *166*(2), 553–573. https://doi.org/10.1111/j.1365-246X.2006.03015.x
Crosby, A., White, N., Edwards, G., Thompson, M., Corfield, R., & Mackay, L. (2011). Evolution of deep-water rifted margins: Testing depth-dependent extensional models. *Tectonics*, *30*, TC1004. https://doi.org/10.1029/2010TC002687

Crosby, A. G., & McKenzie, D. (2009). An analysis of young ocean depth, gravity and global residual topography. *Geophysical Journal International*, *178*(3), 1198–1219. https://doi.org/10.1111/j.1365-246X.2009.04224.x

Divins, D. (2003). *Total sediment thickness of the world's oceans and marginal seas*. Boulder, CO: NOAA National Geophysical Data Center.

Divins, D., & Rabinowitz, P. (1990). Thickness of sedimentary cover for the South Atlantic. In G. B. Udintsev (Ed.), *International geological-geophysical atlas of the Atlantic Ocean*, (pp. 126–127). Moscow: Intergovernmental Oceanographic Commission.

Dutkiewicz, A., Müller, R. D., Hogg, A. M., & Spence, P. (2016). Vigorous deep-sea currents cause global anomaly in sediment accumulation in the Southern Ocean. *Geology*, *44*(8), 663–666. https://doi.org/10.1130/G38143.1

Dutkiewicz, A., O'Callaghan, S., & Müller, R. (2016). Controls on the distribution of deep-sea sediments. *Geochemistry, Geophysics, Geosystems*, *17*, 3075–3098. https://doi.org/10.1002/2016GC006428

Ebbing, J., & Olesen, O. (2010). New compilation of top basement and basement thickness for the Norwegian continental shelf reveals the segmentation of the passive margin system. Paper presented at the Geological Society, London, Petroleum Geology Conference Series 7, 1, 885, 897, DOI: https://doi.org/10.1144/0070885

Funck, T., Geissler, W. H., Kimbell, G. S., Gradmann, S., Erlendsson, Ö., McDermott, K., & Petersen, U. K. (2017). Moho and basement depth in the NE Atlantic Ocean based on seismic refraction data and receiver functions. *Geological Society, London, Special Publications*, *447*(1), 207–231. https://doi.org/10.1144/SP447.1

Gaina, C., Hinsbergen, D. J., & Spakman, W. (2015). Tectonic interactions between India and Arabia since the Jurassic reconstructed from marine geophysics, ophiolite geology, and seismic tomography. *Tectonics*, *34*, 875–906. https://doi.org/10.1002/2014TC003780

Gaina, C., & Jakob, J. (2018). Global Eocene tectonic unrest: Possible causes and effects around the North American plate. *Tectonophysics*. https://doi.org/10.1016/j.tecto.2018.08.010

Gaina, C., Nasuti, A., Kimbell, G. S., & Blischke, A. (2017). Break-up and seafloor spreading domains in the NE Atlantic. *Geological Society, London, Special Publications*, *447*(1), 393–417. https://doi.org/10.1144/SP447.12

Gaina, C., Torsvik, T. H., van Hinsbergen, D. J., Medvedev, S., Werner, S. C., & Labails, C. (2013). The African Plate: A history of oceanic crust accretion and subduction since the Jurassic. *Tectonophysics*, *604*, 4–25. https://doi.org/10.1016/j.tecto.2013.05.037

Goswami, A., Olson, P., Hinnov, L., & Gnanadesikan, A. (2015). OESbathy version 1.0: A method for reconstructing ocean bathymetry with generalized continental shelf-slope-rise structures. *Geoscientific Model Development*, *8*(9), 2735–2748. https://doi.org/10.5194/gmd-8-2735-2015

Grobys, J., Gohl, K., Davy, B., Uenzelmann-Neben, G., Deen, T., & Barker, D. (2007). Is the Bounty Trough off eastern New Zealand an aborted rift? *Journal of Geophysical Research*, *112*, B03103. https://doi.org/10.1029/2005JB004229

Hayes, D. E., & LaBrecque, J. L. (1991). Sediment Isopachs: Circum-Antarctic to 30S. In D. E. Hayes (Ed.), *Marine geological and geophysical atlas of the circum-Antarctic to 30S*, (pp. 29–33). Washington, DC: American Geophysical Union. https://doi.org/10.1029/AR054p0029

Hopper, J. R., Funck, T., Stoker, T., Arting, U., Peron-Pinvidic, G., Doornenbal, J. C., & and C. Gaina, (2014). *Tectonostratigraphic atlas of the north-east Atlantic region*. 340 pp., GEUS, Copenhagen, Denmark.

Horn, M., & Uenzelmann-Neben, G. (2015). The deep Western boundary current at the Bounty Trough, east of New Zealand: Indications for its activity already before the opening of the Tasmanian Gateway. *Marine Geology*, *362*, 60–75. https://doi.org/10.1016/j.margeo.2015.01.011

Huang, X., Gohl, K., & Jokat, W. (2014). Variability in Cenozoic sedimentation and paleo-water depths of the Weddell Sea basin related to pre-glacial and glacial conditions of Antarctica. *Global and Planetary Change*, *118*, 25–41. https://doi.org/10.1016/j.gloplacha.2014.03.010

Jokat, W., & Herter, U. (2016). Jurassic failed rift system below the Filchner-Ronne-shelf, Antarctica: New evidence from geophysical data. *Tectonophysics*, *688*, 65–83. https://doi.org/10.1016/j.tecto.2016.09.018

Jones, S. M., White, N., Clarke, B. J., Rowley, E., & Gallagher, K. (2002). Present and past influence of the Iceland Plume on sedimentation. *Geological Society, London, Special Publications*, *196*(1), 13–25. https://doi.org/10.1144/gsl.sp.2002.196.01.02

LaRowe, D. E., Burwicz, E., Arndt, S., Dale, A. W., & Amend, J. P. (2017). Temperature and volume of global marine sediments. *Geology*, *45*(3), 275–278. https://doi.org/10.1130/G38601.1

Laske, G. (1997). A global digital map of sediment thickness. *Eos, Transactions American Geophysical Union*, *78*, F483.

Laske, G., Masters, G., Ma, Z., & Pasyanos, M. (2013). Update on CRUST1. 0—A 1-degree global model of Earth's crust. Paper presented at the Geophys. Res. Abstracts.

Lindeque, A., Gohl, K., Wobbe, F., & Uenzelmann-Neben, G. (2016). Preglacial to glacial sediment thickness grids for the Southern Pacific Margin of West Antarctica. *Geochemistry, Geophysics, Geosystems*, *17*, 4276–4285. https://doi.org/10.1002/2016GC006401

Ludwig, W., & Houtz, R. (1979). Isopach map of the sediments in the Pacific Ocean Basin, color map with text. American Association of Petroleum Geologists, Tulsa, Okla, USA.

Matthews, K. J., Maloney, K. T., Zahirovic, S., Williams, S. E., Seton, M., & Müller, R. D. (2016). Global plate boundary evolution and kinematics since the late Paleozoic. *Global and Planetary Change*, *146*, 226–250. https://doi.org/10.1016/j.gloplacha.2016.10.002

Matthias, P. K., P.D. Rabinowitz, and N. Dipiazza. (1988). Sediment thickness map of the Indian Ocean, map 505. Am. Assoc. Pet. Geol., Tulsa, OK.

Mitchell, N. C., & Lyle, M. W. (2005). Patchy deposits of Cenozoic pelagic sediments in the Central Pacific. *Geology*, *33*(1), 49–52. https://doi.org/10.1130/G21134.1

Mitchell, N. C., Lyle, M. W., Knappenberger, M. B., & Liberty, L. M. (2003). Lower Miocene to present stratigraphy of the equatorial Pacific sediment bulge and carbonate dissolution anomalies. *Paleoceanography*, *18*(2), 1038. https://doi.org/10.1029/2002PA000828

Molinari, I., & Morelli, A. (2011). EPcrust: A reference crustal model for the European Plate. *Geophysical Journal International*, *185*(1), 352–364. https://doi.org/10.1111/j.1365-246X.2011.04940.x

Morgan, W. J. (1971). Convection plumes in the lower mantle. *Nature*, *230*(5288), 42–43. https://doi.org/10.1038/230042a0

Müller, R. D., Sdrolias, M., Gaina, C., & Roest, W. R. (2008). Age, spreading rates, and spreading asymmetry of the world's ocean crust. *Geochemistry, Geophysics, Geosystems*, *9*, Q04006. https://doi.org/10.1029/2007GC001743

Müller, R. D., Sdrolias, M., Gaina, C., Steinberger, B., & Heine, C. (2008). Long-term sea-level fluctuations driven by ocean basin dynamics. *Science*, *319*(5868), 1357–1362. https://doi.org/10.1126/science.1151540

Müller, R. D., Seton, M., Zahirovic, S., Williams, S. E., Matthews, K. J., Wright, N. M., et al. (2016). Ocean basin evolution and global-scale plate reorganization events since Pangea breakup. *Annual Review of Earth and Planetary Sciences*, *44*(1), 107–138. https://doi.org/10.1146/annurev-earth-060115-012211

Nikishin, A., Gaina, C., Petrov, E., Malyshev, N., & Freiman, S. (2017). Eurasia Basin and Gakkel Ridge, Arctic Ocean: Crustal asymmetry, ultra-slow spreading and continental rifting revealed by new seismic data. *Tectonophysics*, 1–19.

Oakey, G., & Stark, A. (1995). *A digital compilation of depth to basement and sediment thickness for the North Atlantic and adjacent coastal land areas*, (Vol. 3039). Natural Resources Canada.

Olson, P., Reynolds, E., Hinnov, L., & Goswami, A. (2016). Variation of ocean sediment thickness with crustal age. *Geochemistry, Geophysics, Geosystems*, *17*, 1349–1369. https://doi.org/10.1002/2015GC006143

Parsons, B., & Sclater, J. G. (1977). An analysis of the variation of ocean floor bathymetry and heat flow with age. *Journal of Geophysical Research*, *82*(5), 803–827. https://doi.org/10.1029/JB082i005p00803

Péron-Pinvidic, G., Hopper, J. R., Stoker, M., Gaina, C., Funck, T., Árting, U. E., & Doornenbal, J. C. (2017). The NE Atlantic region: A reappraisal of crustal structure, tectonostratigraphy and magmatic evolution—An introduction to the NAG-TEC project. *Geological Society, London, Special Publications*, *447*, 1–9.

Petrov, O., Morozov, A., Shokalsky, S., Kashubin, S., Artemieva, I. M., Sobolev, N., et al. (2016). Crustal structure and tectonic model of the Arctic region. *Earth-Science Reviews*, *154*, 29–71. https://doi.org/10.1016/j.earscirev.2015.11.013

Rebesco, M., Hernández-Molina, F. J., van Rooij, D., & Wåhlin, A. (2014). Contourites and associated sediments controlled by deep-water circulation processes: State-of-the-art and future considerations. *Marine Geology*, *352*, 111–154. https://doi.org/10.1016/j.margeo.2014.03.011

Rogenhagen, J., Jokat, W., Hinz, K., & Kristoffersen, Y. (2004). Improved seismic stratigraphy of the Mesozoic Weddell Sea. *Marine Geophysical Researches*, *25*(3–4), 265–282. https://doi.org/10.1007/s11001-005-1335-y

Schubert, G., & Sandwell, D. (1989). Crustal volumes of the continents and of oceanic and continental submarine plateaus. *Earth and Planetary Science Letters*, *92*(2), 234–246. https://doi.org/10.1016/0012-821X(89)90049-6

Seton, M., Müller, R. D., Zahirovic, S., Gaina, C., Torsvik, T., Shephard, G., et al. (2012). Global continental and ocean basin reconstructions since 200Ma. *Earth-Science Reviews*, *113*(3-4), 212–270. https://doi.org/10.1016/j.earscirev.2012.03.002

Silsbe, G. M., & Malkin, S. Y. (2016). Where light and nutrients collide: The global distribution and activity of subsurface chlorophyll maximum layers. In *Aquatic Microbial Ecology and Biogeochemistry: A Dual Perspective*, (pp. 141–152). Springer.

Stein, C. A., & Stein, S. (1992). A model for the global variation in oceanic depth and heat flow with lithospheric age. *Nature*, *359*(6391), 123–129. https://doi.org/10.1038/359123a0

Sykes, T., Royer, J.-Y., Ramsay, A., & Kidd, R. (1998). Southern hemisphere palaeobathymetry. *Geological Society, London, Special Publications*, *131*(1), 1–42. https://doi.org/10.1144/GSL.SP.1998.131.01.02

Sykes, T. J. S. (1996). A correction for sediment load upon the ocean floor: Uniform versus varying sediment density estimations—Implications for isostatic correction. *Marine Geology*, *133*(1–2), 35–49. https://doi.org/10.1016/0025-3227(96)00016-3

Tominaga, M., Lyle, M., & Mitchell, N. C. (2011). Seismic interpretation of pelagic sedimentation regimes in the 18–53 Ma eastern equatorial Pacific: Basin-scale sedimentation and infilling of abyssal valleys. *Geochemistry, Geophysics, Geosystems*, *12*, Q03004. https://doi.org/10.1029/2010GC003347

Torsvik, T. H., & Cocks, L. R. M. (2016). Tectonic units of the Earth. In L. R. M. Cocks, & T. H. Torsvik (Eds.), *Earth history and palaeogeography*, (pp. 38–76). Cambridge, UK: Cambridge University Press.

Torsvik, T. H., Smethurst, M. A., Burke, K., & Steinberger, B. (2006). Large igneous provinces generated from the margins of the large low-velocity provinces in the deep mantle. *Geophysical Journal International*, *167*(3), 1447–1460. https://doi.org/10.1111/j.1365-246X.2006.03158.x

Udintsev, G. (2003). International geological-geophysical atlas of the Pacific Ocean. Intergovernmental Oceanographic Commission, Moscow-Saint Petersburg.

Uitz, J., Claustre, H., Morel, A., & Hooker, S. B. (2006). Vertical distribution of phytoplankton communities in open ocean: An assessment based on surface chlorophyll. *Journal of Geophysical Research*, *111*, C08005. https://doi.org/10.1029/2005JC003207

Weatherall, P., Marks, K. M., Jakobsson, M., Schmitt, T., Tani, S., Arndt, J. E., et al. (2015). A new digital bathymetric model of the world's oceans. *Earth and Space Science*, *2*, 331–345. https://doi.org/10.1002/2015EA000107

Wessel, P., Smith, W. H., Scharroo, R., Luis, J., & Wobbe, F. (2013). Generic mapping tools: Improved version released. *Eos, Transactions American Geophysical Union*, *94*(45), 409–410. https://doi.org/10.1002/2013EO450001

Whittaker, J. M., Goncharov, A., Williams, S. E., Müller, R. D., & Leitchenkov, G. (2013). Global sediment thickness data set updated for the Australian-Antarctic Southern Ocean. *Geochemistry, Geophysics, Geosystems*, *14*, 3297–3305. https://doi.org/10.1002/ggge.20181

Wobbe, F., Lindeque, A., & Gohl, K. (2014). Anomalous South Pacific lithosphere dynamics derived from new total sediment thickness estimates off the West Antarctic margin. *Global and Planetary Change*, *123*, 139–149. https://doi.org/10.1016/j.gloplacha.2014.09.006